Supporting Information

Mechanism of Inactivation of Ornithine Aminotransferase by (1*S*,3*S*)-3-Amino-4-(hexafluoropropan-2-ylidenyl)cyclopentane-1-carboxylic Acid

Matthew J. Moschitto,[a] Peter F. Doubleday,[b] Daniel S. Catlin,[c] Neil L. Kelleher,[a,b] Dali Liu,[c] Richard B. Silverman[a,b]

[a] *Department of Chemistry, Center for Molecular Innovation and Drug Discovery, and Center for Developmental Therapeutics, Northwestern University, Evanston, Illinois 60208, United States*

[b] *Department of Molecular Biosciences, Chemistry of Life Processes Institute, Northwestern University, Evanston, Illinois 60208, United States*

[c] *Department of Chemistry and Biochemistry, Loyola University Chicago, Chicago, Illinois 60660, United States*

Table of Contents

	Pages
Synthesis of New Inactivators 19 and 20	**S3-S5**
General Synthetic Method	**S3**
Methyl (Z)-3,3,3-trifluoro-2-((1S,4S)-2-(4-methoxybenzyl)-3-oxo-2-azabicyclo[2.2.1]heptan-6-ylidene)propanoate (**22**)	**S3-S4**
Methyl (Z)-3,3,3-trifluoro-2-((1S,4S)-3-oxo-2-azabicyclo[2.2.1]heptan-6-ylidene)propanoate (24)	**S4**
(1*S*,3*S*,*Z*)-3-Amino-4-(1,1,1-trifluoro-3-methoxy-3-oxopropan-2-ylidene) cyclopentane-1-carboxylic acid hydrochloride (19)	**S4-S5**
(1*S*,3*S*,*E*)-3-Amino-4-(1,1,1-trifluoro-3-methoxy-3-oxopropan-2-ylidene) cyclopentane-1-carboxylic acid hydrochloride (**20)**	**S5**
Crystal Structure Data	**S5-S7**
Crystal Structure Growth	**S5**
Data Collection and Processing	**S6**
Model Building and Refinement	**S6**
Figure S1. A simulated annealing omit map	**S6**
Table S1. Statistics of crystal structure of *h*OAT-**1**	**S7**
Table S2. PLP-imine-pyridine dihedral angles in PLP-dependent enzymes	**S8**
Molecular Docking	**S8-S9**
Intact Protein Mass Spectrometry	**S8-S9**
Figure S2. Mass spectra of **1** inactivated hOAT and hOAT	**S10**
Figure S3. Mass spectra of **19** inactivated hOAT and hOAT	**S11**
Metabolomics	**S12-S14**
Figure S4. Mass spectra of PLP and PMP standards and their associated ions	**S13**
Figure S5. OAT metabolite sample with 10 equiv of inhibitor	**S14**
Fluoride Ion Release	**S15-S16**
Fluoride Ion Release Assay	**S15**
Figure S6. Calibration curve generated from varying concentrations of NaF	**S15**
Table S3. Calculation of fluoride ion release for **1**	**S16**
Enzyme Assays	**S16-S17**
General Methods	**S16**
Partition Ratio	**S17**
Figure S7. Time dependence plot for **19**	**S16**
Figure S8. Michaelis plot of k_{obs} obtained from Figure S7 for **19**	**S17**
Spectra	**S18-S22**
^{1}H and ^{13}C NMR of **22**	**S18**
^{1}H and ^{13}C NMR of **23**	**S19**
^{1}H and ^{13}C NMR of **24**	**S20**
^{1}H and ^{13}C NMR of **19**	**S21**
^{1}H and ^{13}C NMR of **20**	**S22**
References	**S23-S24**

Synthesis of New Inactivators 19 and 20

General Synthetic Methods

All chemicals were purchased from Sigma Aldrich, Acros Organics, or Matrix Scientific and used without further purification. Anhydrous solvents (THF, CH_2Cl_2, DMF) were purified before use by passing through a column composed of activated alumina and a supported copper redox catalyst. Yields refer to chromatographically and spectroscopically (^{1}H-NMR) homogeneous material. Analytical thin-layer chromatography (TLC) was performed using Merck Silica Gel 60 Å F-254 precoated plates (0.25 mm thickness), and components were visualized by ultraviolet light (254 nm) and/or ceric ammonium molybdate stain. Flash column chromatography was performed on a Teledyne Combiflash Rf Plus automated flash purification system with various Taledyne cartridges (4-80 g, 40-63 μm, 60 Å). Purifications were performed with hexanes and ethyl acetate unless otherwise noted. ^{1}H and ^{13}C NMR spectra were recorded on a Bruker Avance-III NMR spectrometer at 500 MHz and 126 MHz, respectively, in $CDCl_3$ or D_2O. Chemical shifts were reported in ppm; multiplicities are indicated by s = singlet, d = doublet, t = triplet, q = quartet, sep = septet, dd = doublet of doublet, dt = doublet of triplet, m = multiplet, br = broad resonance. Coupling constants 'J' were reported in Hz. High resolution mass spectral data were obtained on an Agilent 6210 LC-TOF spectrometer in the positive ion mode using electrospray ionization with an Agilent G1312A HPLC pump and an Agilent G1367B autoinjector at the Integrated Molecular Structure Education and Research Center (IMSERC), Northwestern University. Analytical HPLC was performed using a reversed-phase Agilent Infinity 1260 HPLC with a Phenomenex Kintex C-18 column (50 x 2.1 mm, 2.6 μm), detecting with UV absorbance at 254 nm.

Methyl (*Z*)-3,3,3-trifluoro-2-((1*S*,4*S*)-2-(4-methoxybenzyl)-3-oxo-2-azabicyclo[2.2.1]heptan-6-ylidene)propanoate (**22**). Ketone **21**[1] (140 mg, 0.57 mmol) and methyl 3,3,3 trifluoropropionate (0.075 mL, 0.68 mmol, 1.2 equiv) were dissolved in CH_2Cl_2 (3 mL) and cooled to 0 °C. $TiCl_4$ (1.1 mL, 1.14 mmol, 2 equiv, 1 M solution in CH_2Cl_2) was added slowly. The reaction was stirred for 3 h at room temperature, then Et_3N (0.40 mL, 2.85 mmol, 5 equiv) was added. The reaction was further stirred for 18 h and then washed with

1 M HCl (2 mL), dried over Na_2SO_4 and concentrated to yield a black oil, which was purified via column chromatography to yield a mixture of **22** (20 mg, 0.054 mmol, 10% yield) and **23 (**20 mg, 0.054 mmol, 10%) as a white solid. The ratio (and yield) of **22** can be increased by shortening the reaction time at each step to 1 h with yields increasing to 20-30%. **22: ^{1}H NMR** (500 MHz, $CDCl_3$) δ 7.25 (m, 2H), 6.96 (m, 2H), 4.90 (d, J = 15.1 Hz, 1H), 4.74 (p, J = 1.5 Hz, 1H), 3.93 (s, 3H), 3.89 (s, 3H), 3.65 (d, J = 15.2 Hz, 1H), 3.07 (dd, J = 1.8, 3.5 Hz, 1H), 2.93 (m, 2H), 2.17 (ddt, J = 1.8, 3.7, 10.3 Hz, 1H), 1.71 (dt, J = 1.6, 10.5 Hz, 1H). **^{13}C NMR** (126 MHz, $CDCl_3$) δ 176.8, 163.3, 160.4, 159.2, 129.3, 128.3, 122.2 (d, J = 274.3 Hz), 117.9 (q, J = 32.2 Hz), 114.1, 60.6 (q, J = 4.2 Hz), 55.3, 52.5, 43.4, 40.6, 35.6. **HRMS** (ESI) calc'd for $C_{18}H_{19}F_3NO_4$ ($M+H^+$): 370.1266, found: 370.1256. **23: ^{1}H NMR** δ 7.25 (d, *J* = 8.6 Hz, 2H), 6.93 (m, 2H), 5.06 (d, *J* = 1.7 Hz, 1H), 4.69 (d, *J* = 15.0 Hz, 1H), 3.99 (d, *J* = 15.0 Hz, 1H), 3.87 (s, 3H), 3.85 (s, 3H), 3.05 (dt, *J* = 1.5, 3.5 Hz, 1H), 2.79 (m, 2H), 2.14 (d, *J* = 10.4 Hz, 1H), 1.65 (dd, *J* = 1.6, 10.2 Hz, 1H). **^{13}C NMR** (126 MHz, $CDCl_3$) δ 176.8, 163.1, 159.5 (d, *J* = 2.4 Hz), 159.2, 129.3, 128.8, 122.5 (d, *J* = 274.5 Hz), 118.7 (q, *J* = 32.7 Hz), 114.0, 61.7, 55.3, 52.5, 44.0, 43.9, 40.2, 33.6. **HRMS** (ESI) calc'd for $C_{18}H_{19}F_3NO_4$ ($M+H^+$): 370.1266, found: 370.1255.

Methyl (*Z*)-3,3,3-trifluoro-2-((1*S*,4*S*)-3-oxo-2-azabicyclo[2.2.1]heptan-6-ylidene)propanoate (24): 22 (665 mg, 1.80 mmol) was dissolved in MeCN (9 mL) and cooled to 0 °C. Ceric ammonium nitrate (3.0 g, 5.40 mmol, 3 equiv) in 3 mL H_2O was added dropwise, and the reaction was stirred for 2 h. Upon completion, the reaction was diluted with H_2O (5 mL) and extracted with ethyl acetate (2 x 10 mL). After drying over Na_2SO_4 and concentrating, the yellow oil was purified by column chromatography to yield **24** (100 mg, 0.4 mmol, 22% yield) as a white powder. **^{1}H NMR** (500 MHz, $CDCl_3$) δ 5.6 (s, 1H), 4.8 (m, 1H), 3.8 (s, 3H), 2.9 (s, 1H), 2.8 (q, *J* = 2.2 Hz, 2H), 2.2 (dt, *J* = 10.3, 2.0 Hz, 1H), 1.7 (dq, *J* = 10.4, 1.7 Hz, 1H). **^{13}C NMR** (126 MHz, $CDCl_3$) δ 179.4, 163.2, 161.8 (q, *J* = 2.0 Hz), 117.5, 58.0 (q, *J* = 4.0 Hz), 52.5, 43.2, 41.3, 34.7. **HRMS** (ESI) calc'd for $C_{10}H_{11}F_3NO_3$ ($M+H^+$): 250.0691, found: 250.0670.

(1*S*,3*S*,*Z*)-3-Amino-4-(1,1,1-trifluoro-3-methoxy-3-oxopropan-2-ylidene)cyclopentane-1-carboxylic acid hydrochloride (19). Compound **19** (100 mg, 0.40 mmol) was dissolved in 4 M HCl in dioxane (1 mL) and H_2O (1 mL) and heated at 70 °C for 1 h. After concentration, the solid was recrystallized from EtOH/Et_2O to yield

25 (90 mg, 0.30 mmol, 74% yield). **^{1}H NMR** (500 MHz, D_2O) δ 4.79 (m, 1H), 3.82 (s, 3H), 3.15 (m, 3H), 2.49 (dt, *J* = 8.4, 15.3 Hz, 1H), 2.23 (dt, *J* = 4.5, 14.9 Hz, 1H). **^{13}C NMR** (126 MHz, D_2O) δ 179.2, 164.3, 157.9, 122.4 (m), 53.4, 52.3, 40.9, 37.1, 33.6. **HRMS** (ESI) calc'd for $C_{10}H_{13}F_3NO_4$ ($M+H^+$): 268.0797, found: 268.0765.

(1*S*,3*S*,*E*)-3-Amino-4-(1,1,1-trifluoro-3-methoxy-3-oxopropan-2-ylidene)cyclopentane-1-carboxylic acid hydrochloride (**20)**. Compound **20** was prepared from **23** similar to that above in a 17% yield (*two steps*). **^{1}H NMR** (500 MHz, D_2O) δ 3.83 (s, 3H), 3.16 (m, 3H), 2.52 (dt, *J* = 7.8, 15.0 Hz, 1H), 2.13 (dt, *J* = 6.3, 13.9 Hz, 1H). **^{13}C NMR** (126 MHz, D_2O) δ 178.5, 164.4, 161.9, 122.8 (q, *J* = 32.8 Hz), 54.0, 53.5, 41.5, 36.3 (d, *J* = 3.5 Hz), 32.5. **HRMS** (ESI) calc'd for $C_{10}H_{13}F_3NO_4$ ($M+J^+$): 268.0797, found: 268.0766.

Crystal Structure Data

Crystal Structure Growth

Freshly prepared enzyme (200 μg) was dialyzed into 50 mM potassium pyrophosphate containing 5 mM α-ketoglutarate at pH 8.0. Compound **1 (**0.5 mg) was added, and the enzyme was inactivated covered with aluminum foil for 12 h. The coupled enzyme assay indicated no activity. After complete inactivation of *h*OAT activity, the purified enzyme sample was concentrated in 50 mM Tricine pH 7.8 to a protein concentration of 7.5 mg/mL and 5 mg/mL. Crystallization was optimized via the hanging drop vapor diffusion method and was set by varying PEG 6000 (6-18%), NaCl (100-200 mM), glycerol (2.5%-5%), with 50 mM Tricine pH 7.8 kept constant. For each well, 2 drops were set in a 1:1 ratio of well:protein solution. One drop contained the higher protein concentration of 7.5 mg/mL and the other drop in the same well was set with the lower protein concentration of 5 mg/mL. Crystals grew at both concentrations of 5 mg/mL and 7.5 mg/mL. The crystals with the best morphology and size were selected for data collection and grew at a protein concentration of 5 mg/mL in wells containing 10% PEG 6000, 200 mM NaCl, 2.5% glycerol. Crystals were transferred to a cryoprotectant solution (well solution supplemented with 30% glycerol) before being flash frozen in liquid nitrogen.

Data Collection and Processing

Monochromatic data were collected at the LS-CAT, Advanced Photon Source (APS) at Argonne National Laboratory (ANL). Diffraction data were collected at a wavelength of 0.98 Å at 100 K using a Mar300 Charge Coupled Device (CCD) detector. Data sets were indexed and integrated using HKL2000[6] suite. Data statistics are summarized in Table S1.

Model Building and Refinement

The *h*OAT structure was solved by molecular replacement using PHASER in the Phenix software suite.[2] The first search model was based on a previously published structure of *h*OAT (PDB Code: 1OAT). The model was rebuilt using COOT,[3] refined using Phenix, and analyzed in COOT and USCF Chimera.[4] Final refinement statistics are reported in Table S1. Structural figures were made in USCF Chimera.

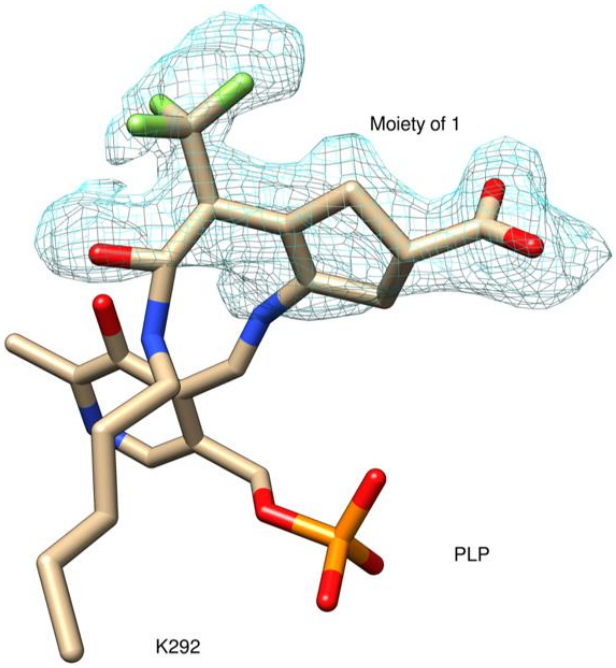

Figure S1. A simulated annealing omit map (F_o-F_c at 2.5 σ) generated by omitting the moiety of **1** while keeping PLP and lys292 was superimposed with the ternary adduct.

Table S1. Statistics of crystal structure of *h*OAT-**1**

Data Processing	
PDB code	6OIA
Space group	P 32 2 $_1$
Cell dimension	
α, β, γ (deg)	90, 90, 120
a, b, c (Å)	115.8 115.8 187.6
Processed Resolution (Å)	1.78
Resolution at I/σ (I) =2 [a]	1.88
R_{merge} [b] (%)	8.7 (117.6) [c]
R_{pim} [d] (%)	3.8 (79.3)
I/σ (I)	17.5 (1.1)
CC ½ [e] (%)	(33.7)
Completeness (%)	97.0 (99.0)
Multiplicity	5.9
No. Reflections	803645
No. Unique Reflections	135892
Refinement	
R_{work} [f]/R_{free} [g] (%)	17.31/20.18
No. of Atoms	
protein	9616
ligand	89
water	1121
B factors (Å^2)	
protein	28.0
RMSD [h]	
bond lengths (Å)	0.004
bond angles (deg)	0.72
Ramachandran plot (%)	
favored	96.27
allowed	3.48
outliers	0.25

[a]Provided Resolution at I/σ = 2 for conventional assessment of data quality
[b]R_{merge} = Σ|Iobs − Iavg|/ΣIavg
[c]The values for the highest-resolution bin are in parentheses
[d]Precision-indicating merging R
[e]Pearson correlation coefficient of two "half" data sets
[f]R_{work} = Σ|Fobs − Fcalc|/ΣFobs
[g]Five percent of the reflection data were selected at random as a test set, and only these data were used to calculate R_{free}
[h]Root-mean square deviation

Table S2. Aminotransferase inhibitors and their dihedral angles derived from crystallography. The dihedral angle is calculated as the angle of deviation of the π-system of the imine bond from the π-system of the pyridinium group.

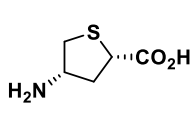

S1

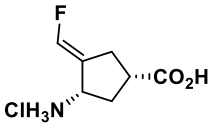

S2

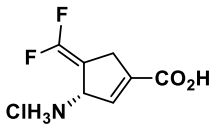

OV329

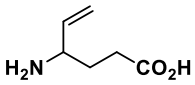

Vigabatrin

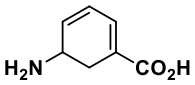

Gabaculine

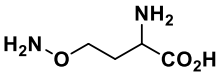

L-Canaline

PDB file	Inhibitor	Enzyme	Dihedral Angle
4y0i	**S1**[5]	GABA-AT	20°
4z5n	**S2**[6]	GABA-AT	33°
6b6g	**OV329**[7]	GABA-AT	30°
1ohw	**Vigabatrin**[8]	GABA-AT	7°
4yod	**CPP-115**[9]	GABA-AT	28°
1gbn	**Gabaculine**[10]	*h*OAT	40°
2can	**L-Canaline**[10]	*h*OAT	50°

Molecular docking

Molecular docking was carried out via a modified literature procedure.[7] The ligands of 5-fluoromethylornithine bound to *h*OAT (2OAT) were removed from the active site. Using the GOLD docking software[11] from Cambridge Crystallographic Data Centre, ligands (as their PLP bound adducts) were docked into the active site using the 5-fluoromethylornithine ligand as a reference. Lys292, Arg413, and Glu235 were allowed to be flexible. The top scored poses were then selected and compared to the initial 5-fluoromethylornithine bound ligand. All renderings were then performed in PyMOL.[12]

Intact protein mass spectrometry

Recombinant *h*OAT and recombinant drug treated *h*OAT were desalted ten times with water on Amicon Ultra 30 kDa molecular weight spin filters (Millipore). To chromatographically resolve OAT, one microgram of protein was loaded onto a 3 cm PLRP-S (Agilent) trap column using a Dionex Ultimate3000 liquid chromatography system (Thermo Fisher). Protein samples were further washed with a 10-min isocratic gradient

of 10% Solvent B (95% MeCN/5% H_2O/0.2% FA) and 90% Solvent A (5% MeCN/95% H_2O/0.2% FA). Protein samples were resolved on an in-house made 75 µm ID x 20 cm long nanobore capillary column packed with PLRP-S resin (Agilent). The LC system was operated at a flow rate of 300 nL/min at the following gradient: 0-10 min 10% Solvent B; 10-12 min to 40% Solvent B; 12-22 min to 90% Solvent B; 22-24 min at 90% Solvent B; 24-26 min to 10% Solvent B; 26-30 min isocratic at 10% Solvent B. Positive mode, full-profile data were acquired in both Orbitrap and ion mass analyzers on a Fusion Lumos Tribrid mass spectrometer (Thermo Fisher) operated in low pressure, protein mode, with a $[M+24H^+]^{+24}$ default charge state. A custom nano-electrospray ionization source was used with a static spray voltage of 1700 V and source fragmentation of 15 V to aid in protein desolvation and ionization. Data were collected in a 500-2,000 *m/z* window, averaging 20 microscans per scan event at a resolving power of 7,500 at (200 *m/z*) with a maximum injection time of 50 ms and a target value for the automatic gain control (AGC) of 5e6 charges for Orbitrap scans. For ion trap scans, the Rapid ion trap scan rate was used with a maximum injection time of 10 ms and an AGC of 3e4 charges.

Summed scans were converted to mzXML format and processed in mMass.[13] Tev protease-cleaved *h*OAT was used for data analysis and the following formulas and mass shifts were examined as single, fixed modification: **43** $C_{17}H_{17}F_3N_2O_8P$, average mass = +465.2952; **43-PLP** $C_9H_6F_3O_4$, average mass = +235.1371. mMass was used to deconvolute individual charge states to generate an average neutral masses. Mass error is reported as the standard deviation from the average mass given independently deconvoluted charge states.

Separately, after desalting, **1** treated recombinant *h*OAT was mixed with trifluoroacetic acid (10 %) and incubated for 12 h at 37 °C. The sample was cooled and filtered using a 30 kDa centrifugal filter. The flow-through was diluted 1:10 in 0.1% formic acid/5% acetonitrile and analyzed for the presence of PLP/PMP (see **Metabolics** section).

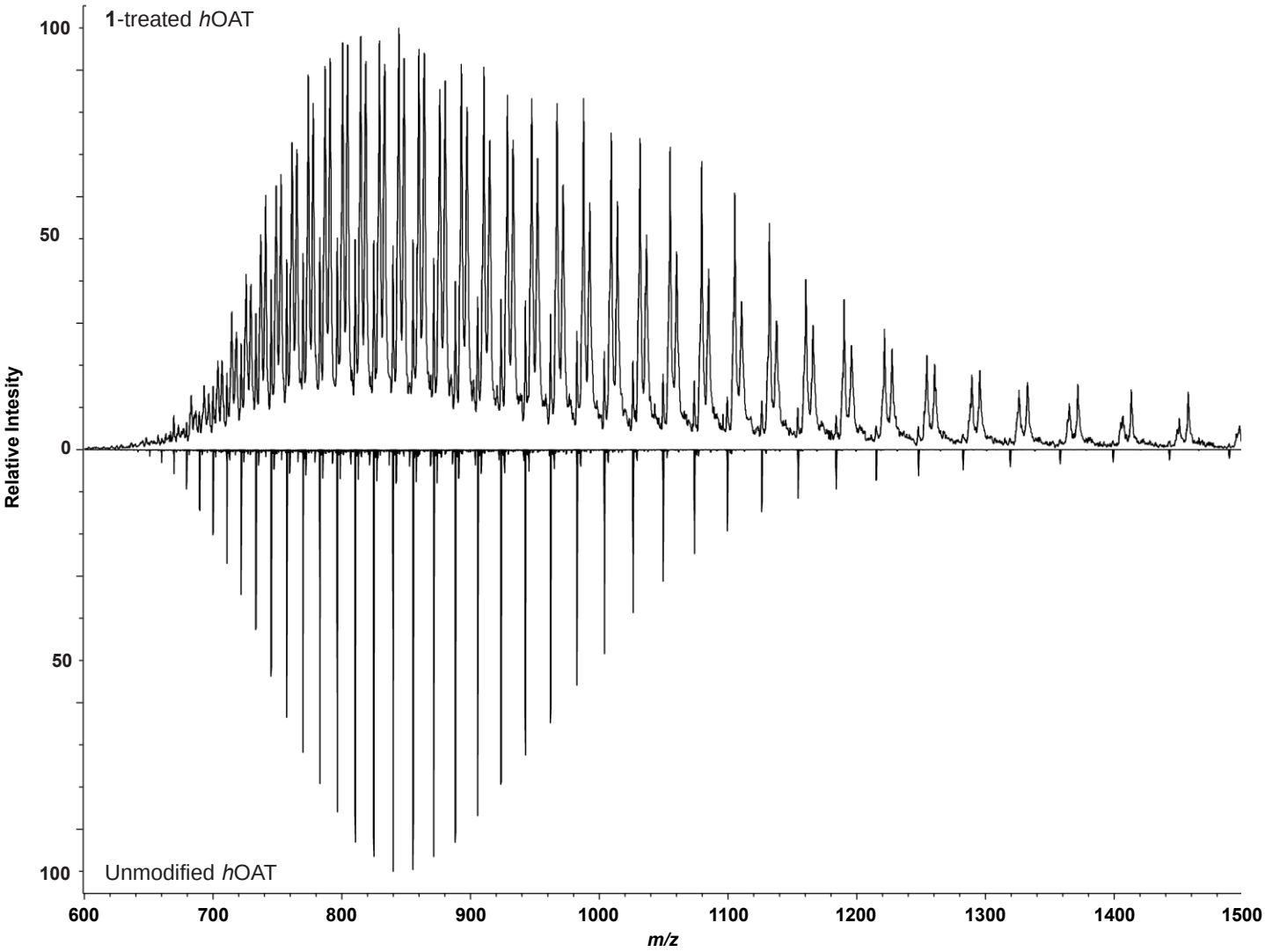

Figure S2. Butterfly plot comparing intact protein mass spectra of intact **1** inactivated hOAT (top) and intact unmodified hOAT (bottom).

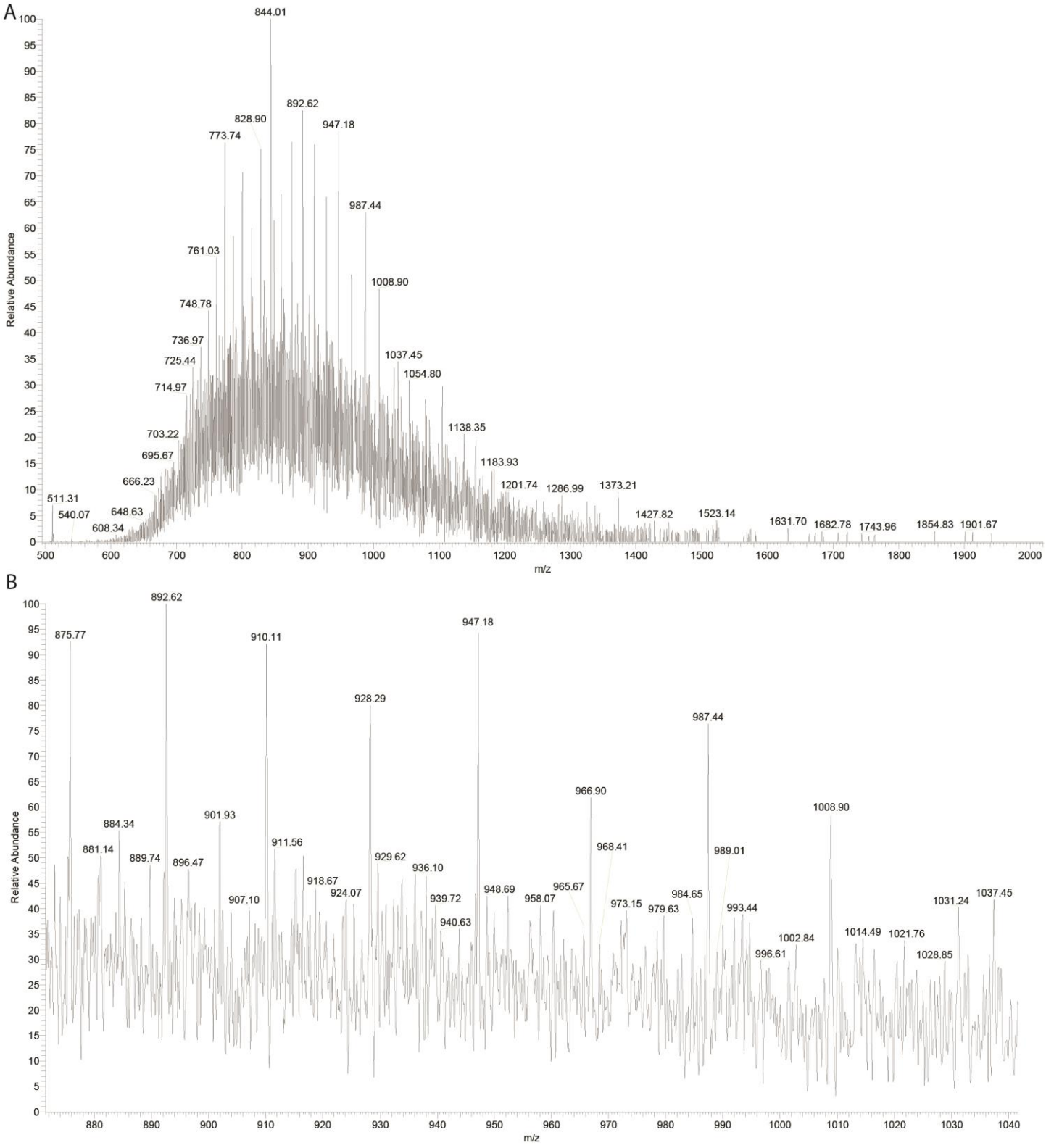

Figure S3: Intact protein mass spectrum for *hOAT* inactivated by **19** (A) and an expanded view of one region showing the corresponding mass and mass shift (B).

Metabolomics

Compound **1 (**20 equiv, 176 μM, double the partition ratio) was dissolved in a 50 mM solution of ammonium bicarbonate at pH 8.0. *h*OAT (20 μg) was added and the volume brought to 50 μL with ammonium bicarbonate solution. The enzyme was inactivated at 23 °C for 3 h. The sample was then spin filtered with an Amicon ultracentrifuge filter (MWCO = 30,000 Da). 20 μL of buffer was added and centrifuged again. The combined flow through samples were diluted 1:10 or 1:20 in Solvent A (5% ACN/95% H_2O/0.2% FA) and injected onto a Kinetex 1.3 μM, 100Å C18 column on an Agilent 1290 Infinity II UHPLC system at 0.7 mL/min, in line with a Thermo Q-Exactive mass spectrometer at a monotonously increasing gradient of Solvent B (95% ACN/5% H_2O/0.2 %FA). Negative and positive ionization mode LC-MS/MS data were separately collected to confidently identify imine and ketone compounds. Negative ESI source parameters are as follows: sheath gas 70, 2.7 kV source ionization voltage and capillary temperature of 320 ºC. A heated ESI source was used at a probe temperature of 275 ºC. Positive-mode ESI data were collected with the HESI source set to 3.4 kV, 70 sheath gas, 275 ºC probe temperature and 320 ºC inlet capillary temperature. Untargeted data-dependent and targeted MS/MS data were collected with HCD fragmentation with a normalized collisional energy, NCE, of 35. For untargeted data-dependent methods the instrument was run with the following MS1 parameters: automatic gain control (AGC) = 1e6 charges, Resolution = 17,500, 40 ms maximum injection time, scanning from *m/z* 100-1000. Tandem MS data were acquired in a data-dependent fashion on the five most abundant precursor ions with a 2 *m/z* precursor isolation window, a minimum AGC target of 6e4, and dynamic exclusion of previously fragmented precursors set to 4 s. Targeted data were collected at a resolution of 35,000, a MS1 AGC target value of 5e4 charges, a maximum injection time of 100 ms, in a 4 *m/z* precursor isolation window, a MS/MS AGC target of 1e5 charges, and 8e3 charges as a lower threshold for MS/MS events.

For PLP/PMP analysis, the ion species of *m/z* 275.01484 and *m/z* 257.02426 $[M-H]^{-1}$ were monitored with the targeted method above. Full MS1-only data were acquired from *m/z* 100-1000 with an AGC of 1e6 and resolution of 17,500 with an 80 ms maximum injection time.

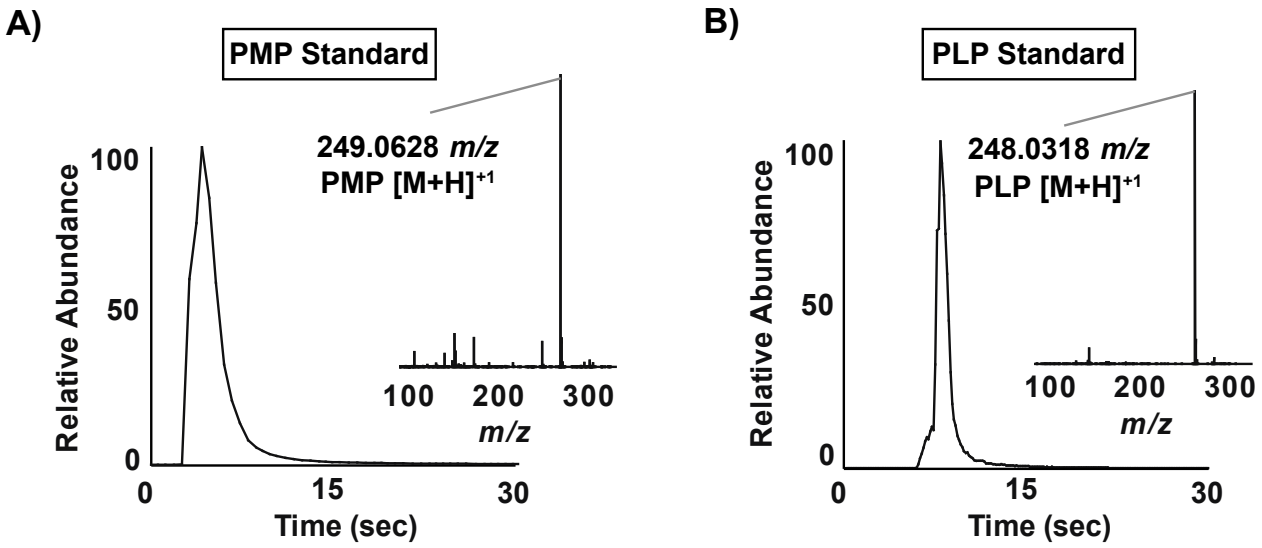

Figure S4. Mass spectra of PMP and PLP standards and their associated ions (inset).

Differential metabolite identification and MS/MS

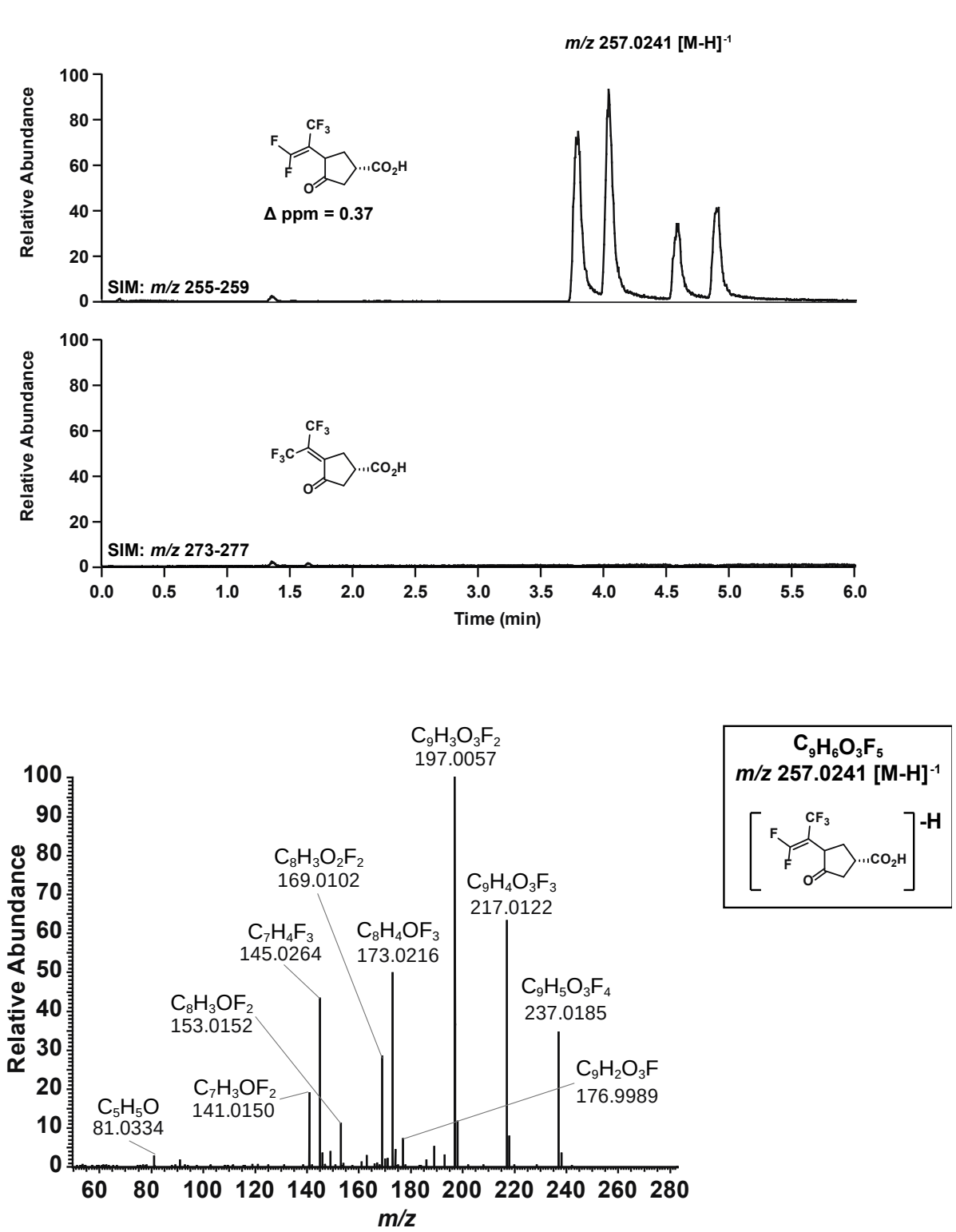

Figure S5. OAT metabolite sample with 10 equiv. of inhibitor was run in (-) ESI mode to selectively monitor ions at A) 255-259 *m/z* (top panel) and 273-277 *m/z* (bottom panel). Only the compound corresponding to the mass 258.0315 Da, and not 276.0221 Da, was identified. Data from each SIM scan are presented at the same fixed relative intensity (NL=1e6). B) HCD (NCE = 35) MS/MS spectra of *m/z* 257.0241 was acquired to confirm metabolite structure.

Fluoride Ion Release

Fluoride Ion Release Assay

The fluoride ion release assay was performed according to literature procedure.[9] Inhibitor (2 mM) was added to a 50 mM solution of potassium pyrophosphate at pH 8.0, and *h*OAT (100 μg) was added. A control containing solely *h*OAT in potassium pyrophosphate buffer was also employed. Enzyme and inhibitor were incubated at 37 °C for 1 h and assayed to ensure no activity. 100 μL of solution was removed from the enzyme-inhibitor sample and added to 1900 μL of TISAB II (57 mL AcOH, 58 g NaCl, 500 mL H_2O at pH 5.5, then diluted to 1 L) containing 0.3 μM fluoride. The probe was immersed in the solution, and the voltage was read after an equilibration time of 5 min. The control sample was then processed in the same manner. Six replicates were performed. Using a calibration curve (Figure S6) and following previous procedures, the number of fluoride ions released per active site was calculated (Table S2).

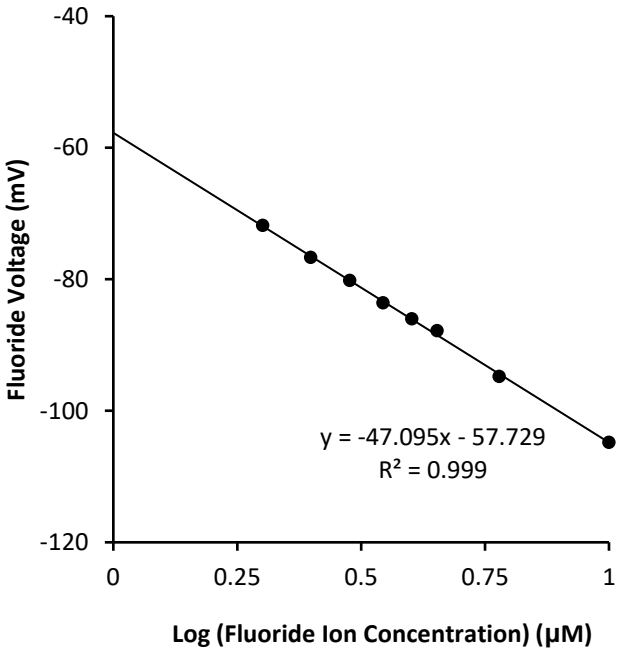

Figure S6. Calibration curve generated from varying concentrations of NaF

Table S3. Calculation of fluoride release for **1**. Tests were run in quadruplicate alternating between Sample reading and Control reading. See methods section for exact procedure.

Entry	Variable	unit	operation	Trial 1	Trial 2	Trial 3	Trail 4
Sample	**S**	**mV**	**From Probe Reading**	**-98.5**	**-97.9**	**-96.9**	**-96.5**
Control	**C**	**mV**	**From Probe Reading**	**-83.8**	**-82.6**	**-79.1**	**-79.6**
Difference	D	mV	S - C	14.7	15.3	17.8	16.9
Sample Concentration	[S]	uM	10^((S+57.729)/-47.095)	7.34	7.13	6.79	6.66
Control Concentration	[C]	uM	10^((C+57.729)/-47.095)	3.58	3.37	2.84	2.91
Concentration of Fluoride detected	[F]	uM	[S]-[C]	3.76	3.75	3.94	3.74
Moles F-	F	mol	[F] x 0.002L	7.53E-09	7.51E-09	7.89E-09	7.49E-09
original F- moles	F_n	mol	F x 5.1 (dilution)	3.84E-08	3.83E-08	4.02E-08	3.82E-08
mg enzyme	E	g	0.2 mL x 0.11 mg/mL	2.20E-05	2.20E-05	2.20E-05	2.20E-05
moles enzyme / active site	E_n	mol	E / 45000	4.89E-10	4.89E-10	4.89E-10	4.89E-10
Fluoride released per active site	F/E		F_n / E_n	78.51	78.33	82.31	78.10

Average Fluoride Released	**79**
Standard Deviation	**2.00**

Enzyme Assays

General Methods

*h*OAT and PYCR1 were expressed, grown, and purified according to literature procedures.[14,15] GABA-AT was isolated from pig brains and purified according to a literature procedure.**Error! Bookmark not defined.** Coupled enzyme assays for GABA-AT and *h*OAT were carried out according to previous procedures.[9,16]

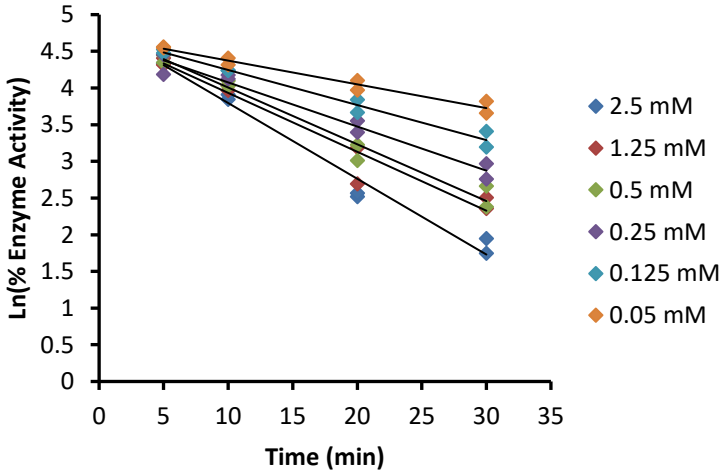

Figure S7. Time dependence plot for **19**. Preincubation time was plotted against the natural log of percent enzyme inhibition for various inhibitor concentrations. The k_{obs} was extracted from the slope of the linear regression.

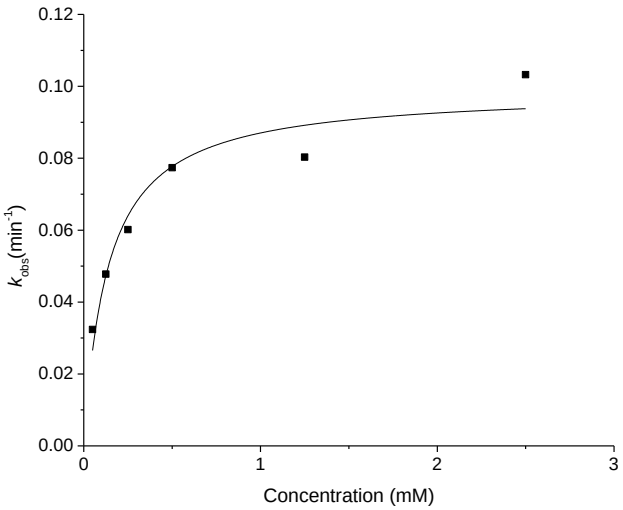

Figure S8. Michaelis plot of k_{obs} obtained from Figure S7 for compound **19**

Partition Ratio

The partition ratio was calculated using previous protocols.[9]

Spectra

^{1}H and ^{13}C NMR of **22**

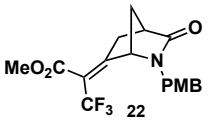

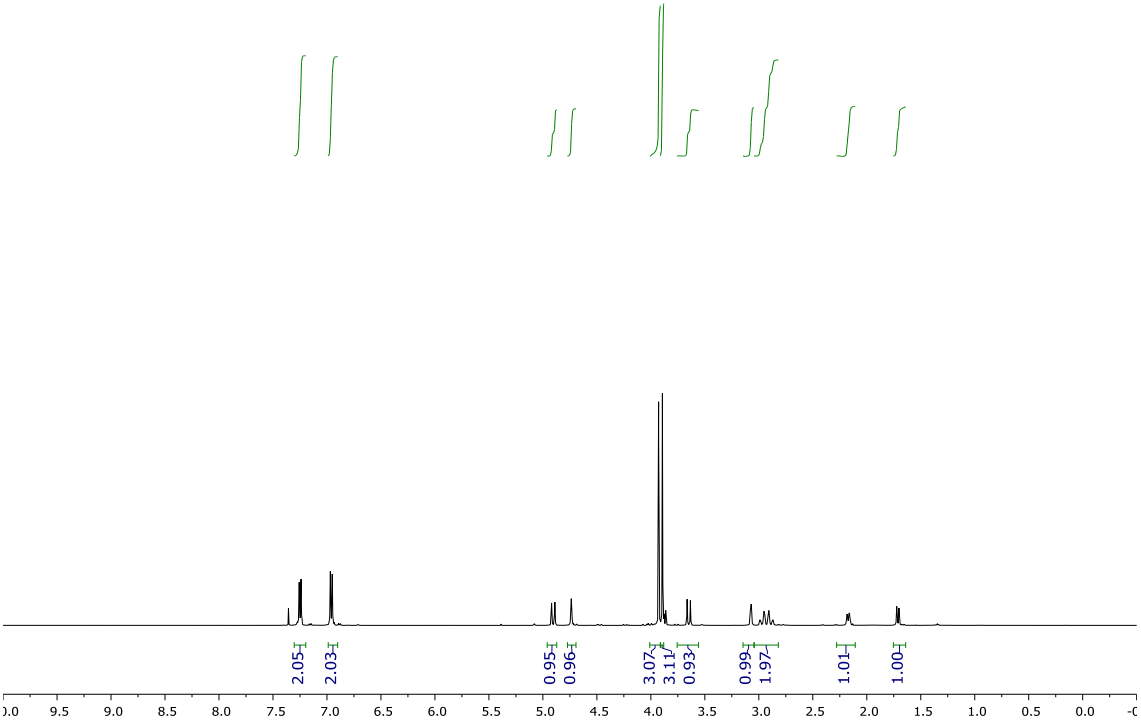

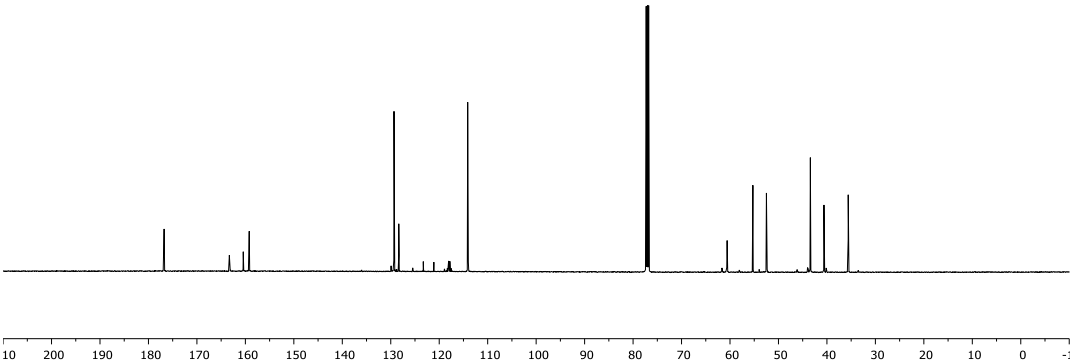

^{1}H and ^{13}C NMR of **23**

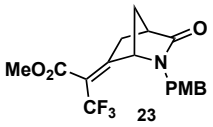

23

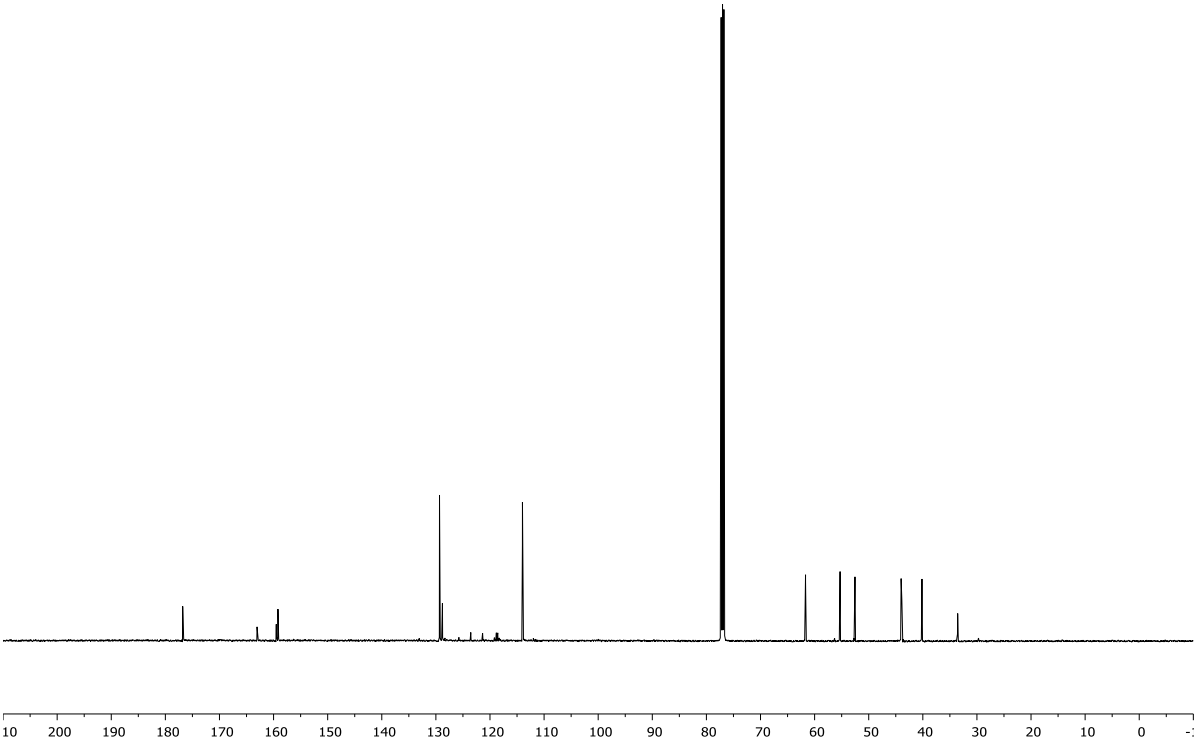

^{1}H and ^{13}C NMR of **24**

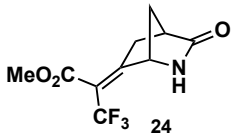

24

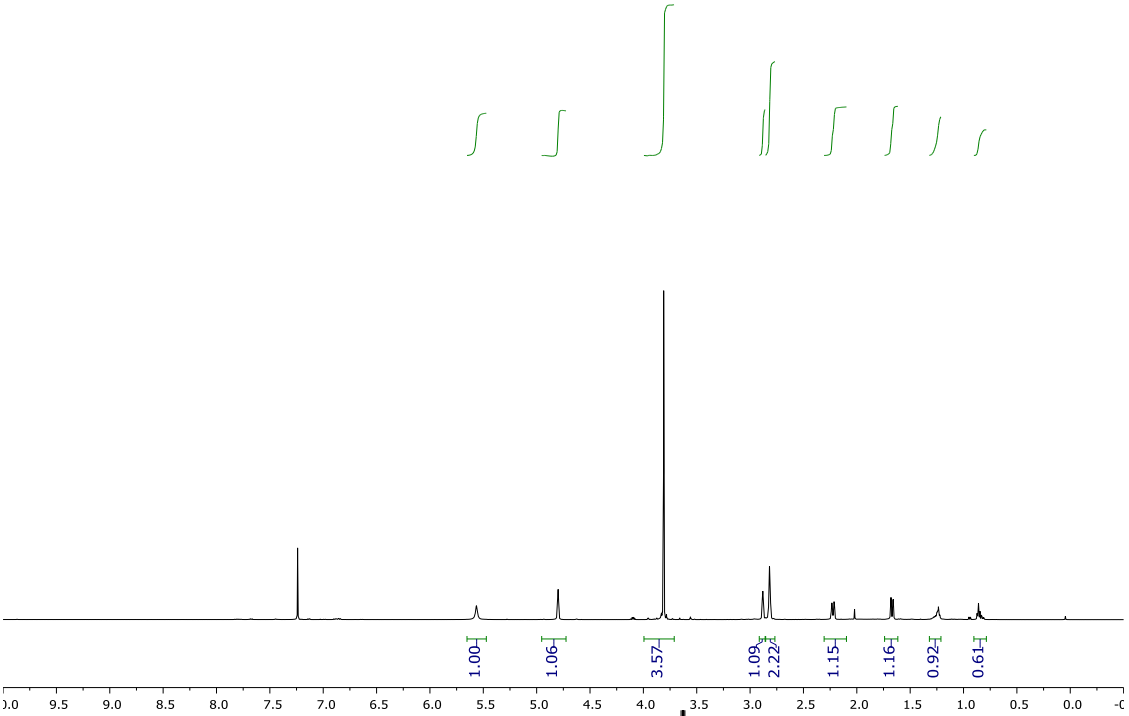

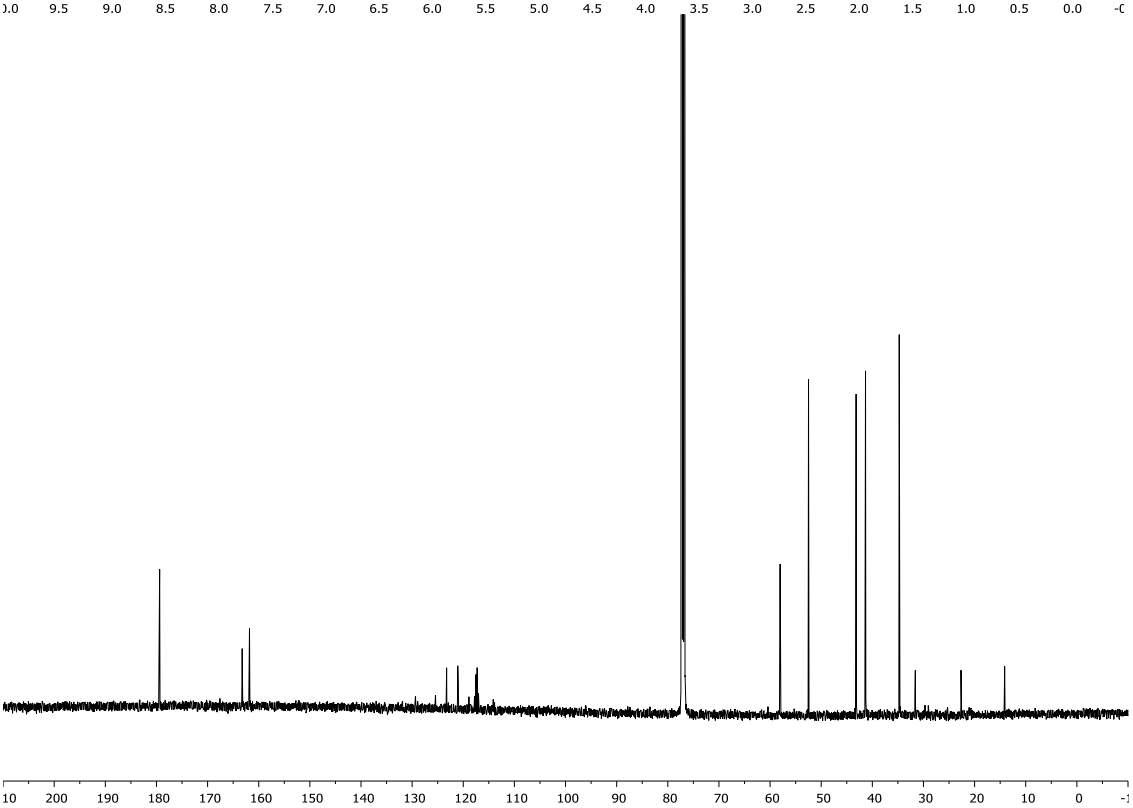

^{1}H and ^{13}C NMR of **19**

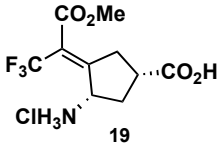

19

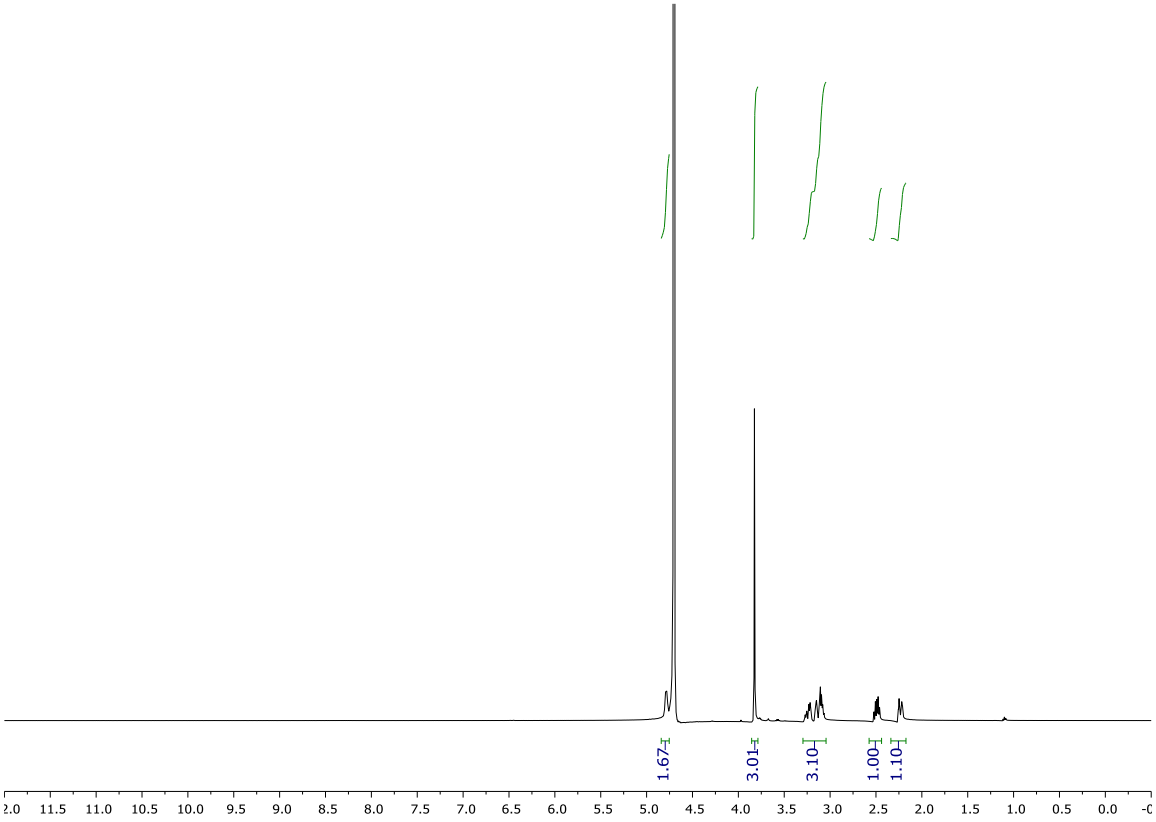

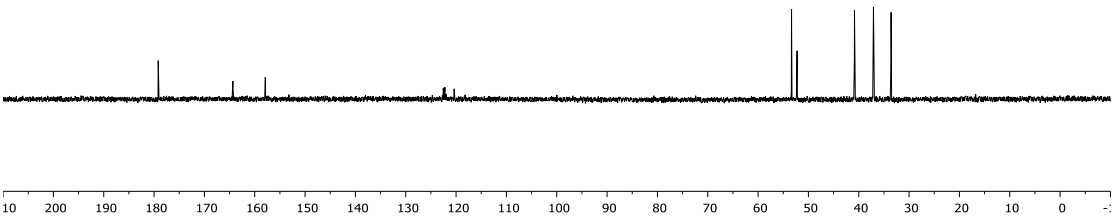

^{1}H and ^{13}C NMR of **20**

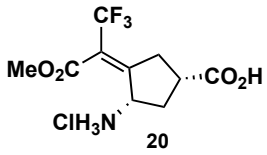

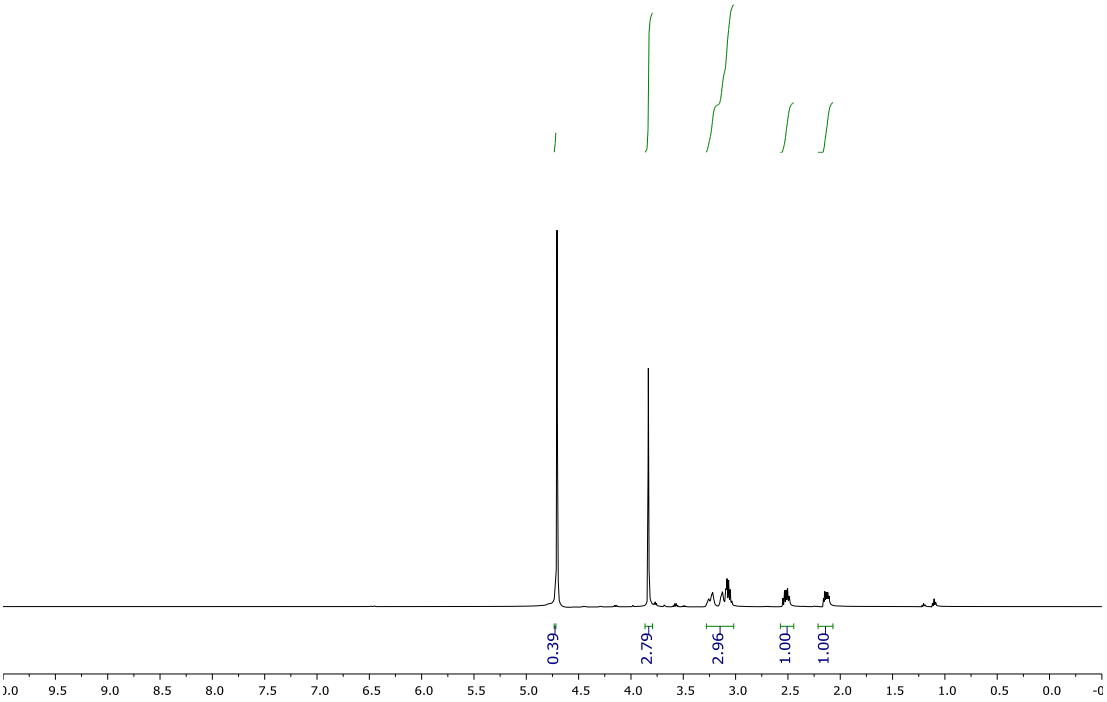

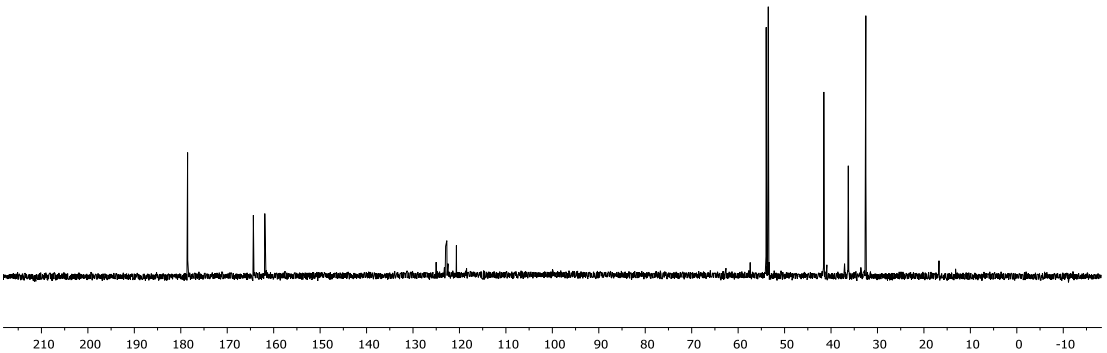

References

[1] Pan, Y.; Qiu, J.; Silverman, R. B. *J. Med. Chem.* **2003**, *46*, 5292-5293.

[2] Adams, P. D.; Afonine, P. V.; Bunkoczi, G.; Chen, V. B.; Davis, I. W.; Echols, N.; Headd, J. J.; Hung, L. W.; Kapral, G. J.; Grosse-Kunstleve, R. W.; McCoy, A. J.; Moriarty, N. W.; Oeffner, R.; Read, R. J.; Richardson, D. C.; Richardson, J. S.; Terwilliger, T. C.; Zwart, P. H. *Acta Crystallogr.D* **2010**, *66*, 213-221.

[3] Emsley, P.; Lohkamp, B.; Scott, W. G.; Cowtan, K. *Acta Crystallogr. D Biol Crystallogr.* **2010**, *66*, 486-501.

[4] Pettersen, E. F.; Goddard, T. D.; Huang, C. C.; Couch, G. S.; Greenblatt, D. M.; Meng, E. C.; Ferrin, T. E. *J. Comput. Chem.* **2004**, *25*, 1605-1612.

[5] Le, H. V.; Hawker, D. D.; Wu, R.; Doud, E.; Widom, J.; Sanishvili, R.; Liu, D.; Kelleher, N. L.; Silverman, R. B. Design and mechanism of tetrahydrothiophene-based gamma-aminobutyric acid aminotransferase inactivators. *J. Am. Chem. Soc.* **2015**, 137, 4525-4533.

[6] Lee, H.; Le, H. V.; Wu, R.; Doud, E.; Sanishvili, R.; Kellie, J. F.; Compton, P. D.; Pachaiyappan, B.; Liu, D.; Kelleher, N. L.; Silverman, R. B. Mechanism of inactivation of gaba aminotransferase by (e)- and (z)-(1s,3s)-3-amino-4-fluoromethylenyl-1-cyclopentanoic acid. *ACS. Chem. Biol.* **2015**, 10, 2087-2098.

[7] Juncosa, J. I.; Takaya, K.; Le, H. V.; Moschitto, M. J.; Weerawarna, P. M.; Mascarenhas, R.; Liu, D.; Dewey, S. L.; Silverman, R. B. Design and mechanism of (s)-3-amino-4-(difluoromethylenyl)cyclopent-1-ene-1-carboxylic acid, a highly potent gamma-aminobutyric acid aminotransferase inactivator for the treatment of addiction. *J. Am. Chem. Soc.* **2018**, 140, 2151-2164.

[8] Storici, P.; De Biase, D.; Bossa, F.; Bruno, S.; Mozzarelli, A.; Peneff, C.; Silverman, R. B.; Schirmer, T. Structures of gamma-aminobutyric acid (gaba) aminotransferase, a pyridoxal 5 '-phosphate, and [2fe-2s] cluster-containing enzyme, complexed with gamma-ethynyl-gaba and with the antiepilepsy drug vigabatrin. *J. Biol. Chem.* **2004**, 279, 363-373.

[9] Lee, H.; Doud, E. H.; Wu, R.; Sanishvili, R.; Juncosa, J. I.; Liu, D.; Kelleher, N. L.; Silverman, R. B. Mechanism of inactivation of gamma-aminobutyric acid aminotransferase by (1S,3S)-3-amino-4-

difluoromethylene-1-cyclopentanoic acid (CPP115). *J. Am. Chem. Soc.* **2015**, 137, 2628-2640.

[10] Shah, S. A.; Shen, B. W.; Brünger, A. T. Human ornithine aminotransferase complexed with l-canaline and gabaculine: Structural basis for substrate recognition. *Structure* **1997**, 5, 1067-1075.

[11] Jones, G.; Willett, P.; Glen, R. C.; Leach, A. R.; Taylor, R. *J. Mol. Biol.* **1997**, *267*, 727-748.

[12] The PyMOL Molecular Graphics System, Version 1.8 Schrödinger, LLC

[13] Niedermeyer, T. H. J.; Strohalm, M. *PLoS One* **2012**, *7*, e44913.

[14] Mascarenhas, R.; Le, H. V.; Clevenger, K. D.; Lehrer, H. J.; Ringe, D.; Kelleher, N. L.; Silverman, R. B.; Liu, D. *Biochemistry* **2017**, *56*, 4951-4961.

[15] Christensen, E. M.; Patel, S. M.; Korasick, D. A.; Campbell, A. C.; Krause, K. L.; Becker, D. F.; Tanner, J. J. *J. Biol. Chem.* **2017**, *292*, 7233-7243.

[16] Juncosa, J. I.; Lee, H.; Silverman, R. B. *Anal Biochem* **2013**, *440*, 145-149.